Acta Crystallographica Section D
Biological Crystallography
ISSN 0907-4449

Conceptions and first results on the electrocrystallization behaviour of ferritin

Abel Moreno[a] and Margarita Rivera[b]*

[a]Instituto de Química, Universidad Nacional Autónoma de México, Mexico, and [b]Instituto de Física, Universidad Nacional Autónoma de México, Mexico

Correspondence e-mail: mrivera@servidor.unam.mx

Received 9 August 2005
Accepted 19 October 2005

The role of electrochemical processes on Fe and $CdSO_4$ in the crystallization of horse spleen ferritin has been investigated using the cyclic voltammetry technique. It was found that although both species exhibit important redox properties in the presence of an external applied potential, $CdSO_4$ played a leading role not only in the nucleation process but also in the growth behaviour and morphology of ferritin crystals.

1. Introduction

A general understanding of protein nucleation and crystal-growth processes is very important for obtaining crystals suitable for X-ray crystallography. Obtaining adequate-sized and high-quality crystals of different metalloproteins for structural investigations is still a challenge in many laboratories. In particular, there are some metals or essential elements (biominerals) that appear in many biological systems which deserve special attention owing to their specific functions in living systems.

Iron, an essential element in living organisms, is commonly used in the Fe^{II} oxidation state. However, in our oxidizing atmosphere, Fe^{III} is the more prevalent oxidation state. At physiological pH, the Fe^{III} ion concentration in aqueous solution is minimal. However, most organisms maintain an intracellular concentration of Fe^{III} that is several orders of magnitude higher than in simple aqueous solutions. This discrepancy in concentration demonstrates the striking ability of biochemical systems to concentrate and store iron. Conversely, iron can be very toxic, so the ability to store and release iron in a controlled fashion is essential. Cells have solved this problem of iron storage by developing ferritins, a family of iron-storage proteins that sequester iron inside a protein coat as a hydrous ferric oxide-phosphate mineral similar in structure to the mineral ferrihydrite.

Ferritin is a spherical shell that consists of 24 units (or peptide chains) folded into ellipsoids. Each subunit is an individual molecule that joins to its neighbouring subunits through non-covalent interactions; the subunits have a combined molecular weight of 474 kDa. These subunits pack to form a hollow sphere approximately 80 Å in diameter with walls that are approximately 10 Å thick. The important structural features of ferritin include the presence of two types of channels that occur in the protein wall at the intersection of the subunits which allow the intake and release of iron from the molecule (Theil, 2001).

Ferritin usually crystallizes in a cubic system. However, this has been found to depend on the precipitating agent; for instance, a tetragonal form can be obtained when sodium chloride is used for this purpose. Additionally, an orthorhombic form is obtained using different concentrations of sodium chloride and different pH values. These crystallographic structures have been compared at high resolution using X-ray methods (Granier *et al.*, 1997). The nucleation phenomena of ferritin and apoferritin have been extensively reviewed by Yau & Vekilov (2001).

Direct electrochemical measurements of metalloproteins have been performed on the surface of metal-oxide electrodes (Harmer *et al.*, 1985). It was found that cyclic voltammetry can be an accurate and

useful technique for application to the electrochemical characterization of metalloproteins and their complexes (Olafson, 1988).

The significant role of electrostatic interactions in the stabilization of protein assemblies as well as their effect on nucleation control and the crystallization process have also been taken into account. For instance, the magnetic properties of ferritin under the influence of a strong magnetic field and its effect upon nucleation and growth of crystals were initially investigated by Sazaki *et al.* (1997) and, more recently, the coupled magnetic and electric effects on lysozyme have been investugated by Sazaki *et al.* (2004). Therefore, the electrochemical properties of ferritin open new possibilities not only to understand the crystallization process but also to observe the role of macromolecular impurities in proteins absorbed onto different substrates such as gold electrodes (Tominaga *et al.*, 2004).

In particular, the intake and release mechanism of iron from ferritin is related to the redox properties of Fe. $CdSO_4$ also exhibits important redox properties and is therefore largely used for the purpose of making standard electric cells. In this work, we have investigated the influence of an external applied potential and the crystal-growth behaviour of ferritin from horse spleen by using the cyclic voltammetry technique on the growth mechanism of ferritin crystals in the presence of $CdSO_4$.

2. Materials and methods

2.1. Protein preparation and characterization

Ferritin from horse spleen was obtained from Sigma–Aldrich (code F4503) and was further purified on a gel-filtration column using HPLC methods with 0.05 *M* sodium acetate pH 5 in order to separate ferritin oligomers.

2.2. Dynamic light-scattering analysis

Dynamic light-scattering (DLS) analysis was performed using a DynaPro-801 from Protein Solutions. All solutions were initially filtered using Anotop filters of 0.20 µm and then 0.020 µm for the monomer characterization. The analysis was performed using the *DYNAMICS* software supplied by Protein Solutions Co. All crystallization experiments were performed using the batch method using a ferritin solution of 22 mg ml^{-1} and 0.25 *M* $CdSO_4$ in a 1:1 molar ratio.

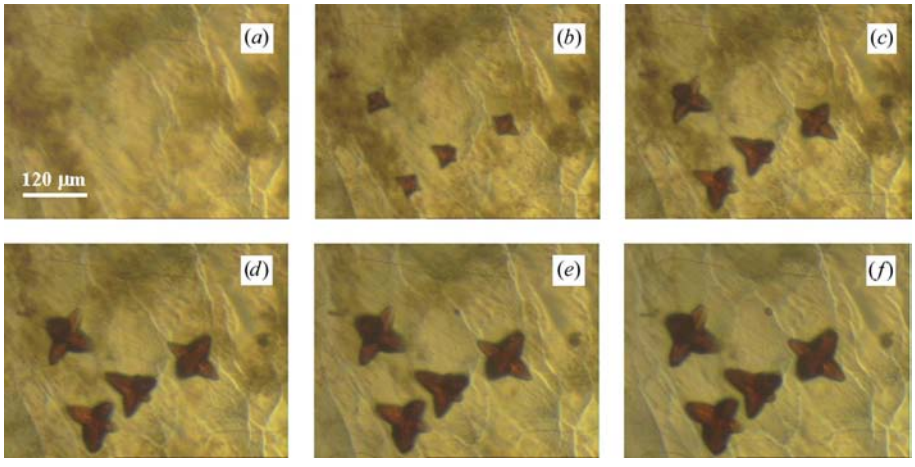

Figure 1
Time-sequence optical images of the HOPG at (*a*) 0, (*b*) 20, (*c*) 40, (*d*) 60, (*e*) 80 and (*f*) 100 min from the beginning of the experiment. Reference system without potential.

2.3. Electrocrystallization and imaging data collection

The electrocrystallization experiments were performed in an electrochemical fluid cell (50 µl) from Digital Instruments (MultiMode SPM, NanoScope IIIa). The cyclic voltammetry characterization was performed using the potentiostat/galvanostat module of the SPM; a triangular-shaped wave potential was employed. In this configuration, a silver wire was used as a reference electrode, a platinum wire as a counter-electrode and a highly oriented pyrolytic graphite (HOPG) surface as a working electrode. The electrochemical potential was cycled between −950 and +500 mV at 40 mV s^{-1} in all cases. The solution under electrochemical control was monitored with a CCD optical video camera coupled to the AFM. The program *AxioVision* provided by Zeiss Co. was used to record the digital images.

2.4. X-ray diffraction and SEM–EDS characterization

X-ray data collection was performed at 113 K using a Rigaku R-AXIS IIc diffractometer with a rotating-anode generator (operated at 50 kV, 100 mA). Additionally, a synchrotron-radiation facility was used in order to obtain high-resolution X-ray data (beamline 12 at NSLS, Brookhaven, NY, USA). The crystals were analysed in a cryosolution containing 60% glycerol in the same precipitating agent solution. Data collection was performed at 113 K in a nitrogen stream collecting 60° of data for 10 s each. One data set was performed for each crystal (control, grown under potential difference and regrown after applying the potential difference). The X-ray data were reduced and integrated using the *CrystalClear* package supplied by Rigaku Co.

The SEM and EDS images were obtained with a Jeol JSM5600 LV microscope coupled with a Noran X-ray microanalysis system. The experiments were carried out at 20 keV at high vacuum.

3. Results and discussion

From the HPLC method, three different ferritin fractions were obtained; the first exhibited the largest radius and molecular weight, while the last exhibited the smallest radius and molecular weight as is usually observed in gel-permeation chromatography. The three fractions were characterized separately by DLS techniques, showing hydrodynamic radii of 60, 40 and 8 nm for the oligomers, tetramers and isolated monomers, respectively. The three populations were properly separated in order to perform further crystallization tests. It is well known that conventional preparation of ferritin from horse spleen produces a heterogeneous material owing to the existence of dimers, trimers and higher oligomers. The nature and origin of ferritin oligomers is still not known. Saeed & Boyde (1981) separated ferritin monomers and the individual polymeric forms by preparative polyacrylamide-gel electrophoresis and found that the formation of oligomers occurs during the crystallization of ferritin monomers.

Crystallization experiments were carried out using the three different fractions at different protein and precipitating-agent ($CdSO_4$) concentrations at room temperature. The chosen values of the concentration and molar ratio were determined by the crystallization response of the mixtures. For

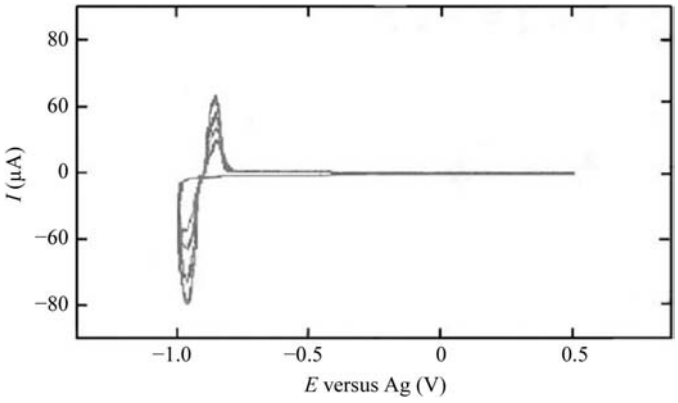

Figure 2
Cyclic voltammetry plot of 22 mg ml^{-1} ferritin and 0.25 *M* $CdSO_4$ mixture in the AFM electrochemical cell. The switching potential interval was +0.5 V, −0.95 V *versus* Ag. The sweep rate was 40 mV s^{-1}.

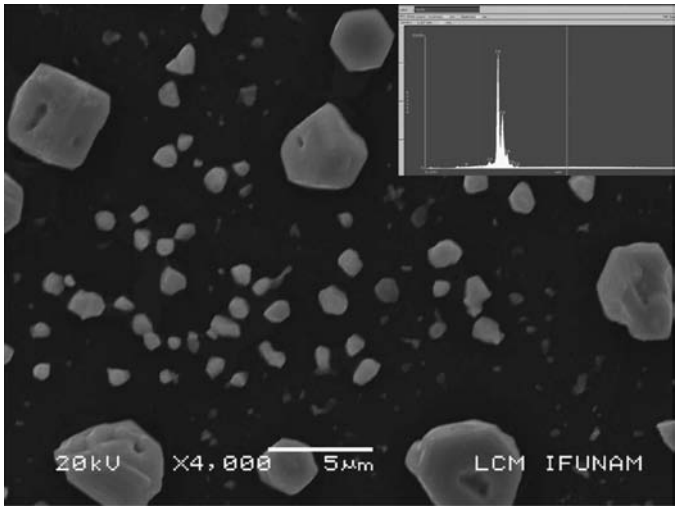

Figure 3
SEM–EDS characterization of Cd crystals grown on the HOPG surface. The inset shows the EDS characterization of the nuclei, where mainly metallic Cd was detected (99.8%) in the majority of the analysed crystals.

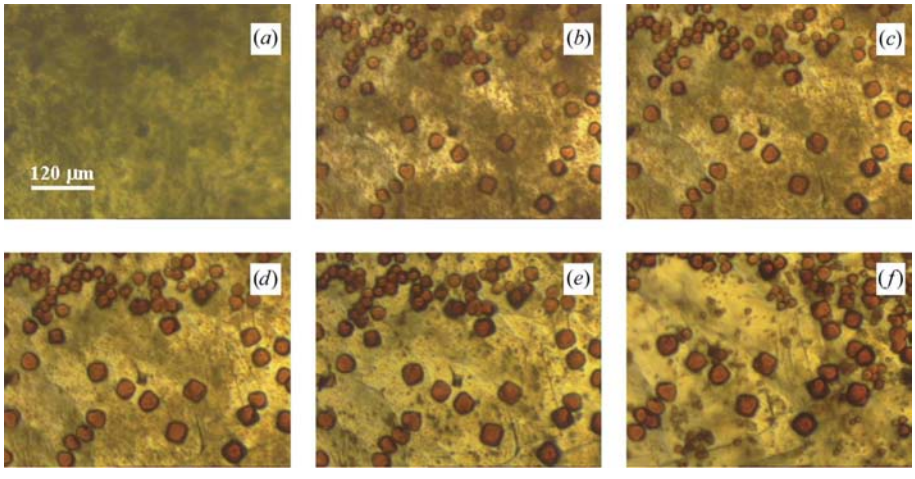

Figure 4
Time-sequence optical images of the HOPG electrode at (*a*) 0, (*b*) 20, (*c*) 40, (*d*) 60, (*e*) 80 and (*f*) 100 min from the beginning of the experiment. The potential was cycled between +0.5 and +0.95 V *versus* Ag at 40 mV s^{-1}.

instance, the best response was obtained for the second fraction, in which tetramers were observed. Under these conditions, the different protein solutions were introduced into the electrochemical fluid cell (50 µl) of a MultiMode SPM/NanoScope IIIa (Digital Instruments). For each concentration, two different experiments were carried out to compare the influence of an applied potential on the growth mechanism of ferritin crystals. One crystal-growth experiment was performed in the absence of an external potential, while another was performed under the influence of an external triangular-shaped potential using the same experimental conditions.

The largest crystals grown under normal conditions were obtained for 22 mg ml^{-1} ferritin and 0.25 *M* $CdSO_4$ at a 1:1 mixture molar ratio. In Fig. 1, time-sequence images of the experiment in the absence of an external potential are observed. Images of the HOPG working electrode in the presence of the electrolyte solution were recorded every 5 min. The first crystals appeared after 10 min. At the beginning they exhibited cubic shapes, but as the time increased they showed four triangular lobes. After 1.5 h, the size and shape of the crystals remained constant. The average face displacement of the crystals after this time was 120 µm.

In Fig. 2, the cyclic voltammetry response of the ferritin–$CdSO_4$ solution is shown. It was observed that the electrochemical ferritin-crystallization process in the presence of $CdSO_4$ is dominated by the $CdSO_4$ redox mechanism in the (+0.5, −0.95) V potential interval, since the plot exhibits the typical redox behaviour of $CdSO_4$ in the absence of the protein solution. From this plot, a crossover typical of the nucleation phenomena and a peak reduction arising from a decrease in the cadmium concentration are observed. Moreover, AFM and SEM images of the HOPG electrode surface show small cadmium aggregates just after the first few potential scan cycles as seen in Fig. 3. The EDS characterization showed 99.8% Cd metallic centres for all the analysed nuclei.

In Fig. 4, the time-sequence evolution of ferritin crystals under the influence of the applied potential is shown. The experiment was followed at regular intervals of 5 min. After 30 min, the size did not change considerably. This fact is particularly interesting because the system itself tries to be in equilibrium after depositing metallic Cd since the initial concentration of Cd^{II} is diminished when the metallic nucleation centres are formed. Consequently, these centres work as templates where ferritin will crystallize. Additionally, the process is almost autoregulated and the crystals will finally be obtained at the proper supersaturation to produce cubic crystals. It is well known that facetted crystals are formed only if the thermal energy, kT, is far from the interfacial energy per molecule since thermal fluctuations destroy the perfect molecular packing of the crystal face. If we apply a well controlled potential difference, the thermal fluctuations will not allow the facetted nucleus to be destroyed and cubic shaped ferritin crystals will then be obtained. Presumably, the opposite situation occurs for the dendrite-shaped crystals in Fig. 1. It is worth mentioning that from the optical images more crystals grew in the potential-controlled experiment than in the reference experiment, although the potential-controlled experiments were smaller. One possible explanation of this phenomenon is related to the presence of a larger quantity of cadmium nuclei on the electrode surface owing to the electrodeposition

process. The experiments were repeated several times and the same trend was observed in all cases.

In order to investigate the growth rate for both different crystals, measurements of the crystal-face displacement *versus* time were performed. It was found that the growth rate was 100 Å s^{-1} for the dendritic crystals in contrast to 18.9 Å s^{-1} for the cubic crystals. Moreover, time-sequence images of the crystals grown at the same time intervals showed that the ferritin crystal shape obtained under the applied potential influence remained cubic for a longer time, while the control system eventually showed dendritic forms. This result might be attributed either to a gradient in the buffer concentration at the working electrode or to buffer-ion mobility at the interface.

In the first case, as the voltage was cycled, $CdSO_4$ was electrodeposited on the electrode surface, decreasing the cadmium concentration at the interface. This cadmium gradient has the appropriate characteristics to sustain the growth of well defined crystal shapes near the working electrode surface. On the other hand, the external applied potential imposes a specific diffusion rate on the free cadmium ions, decreasing the crystal-formation velocity and therefore sustaining cubic shaped crystals for a longer time.

Although it was possible to obtain crystals from both experiments, their size in all cases was unfortunately too small to obtain sufficient X-ray diffraction data using a rotating-anode generator. The X-ray characterization of ferritin crystals was therefore carried out using an X-ray synchrotron source (beamline 12 at Brookhaven National Laboratory, NY, USA). This showed that all crystals were cubic, having space group $F432$ and unit-cell parameter a = 182.37 Å. In all cases there was not any remarkable difference in the statistics in crystal-quality analysis.

It is worth mentioning that the ferritin crystals obtained from the oligomers were mainly dendritic, but were cubic octahedral in some cases; they were only cubic octahedral for the monomer fraction in the presence of an external applied potential. These results were consistently obtained on the surface of the graphite electrode. In our case, when we used the tetramer fraction we observed cubic shaped single crystals which probably resemble the cubic structure of the metal (cadmium) template. Additionally, from crystal-growth theory, it is plausible to say that there is kinetic control of the crystallization process when the potential difference is applied for this case.

Another interesting feature was observed from the experiments when the previous crystals were used as seeds in order to increase their size. For this purpose, a fresh drop of ferritin–$CdSO_4$ solution was added to the crystals on the working-electrode surface. In general, a week later the crystals exhibited slightly larger sizes. Furthermore, although the non-potential-grown crystals from the tetramer fraction originally exhibited dendritic shapes when the fresh solution was added, after a few days some of the crystals began to show cubic shapes.

4. Conclusions

These promising results show the effect of an external applied potential to trigger well defined cubic shaped crystals when the nucleation of cadmium centres is controlled using this voltammetric method. Future work will be focused on the growth mechanism of suitable ferritin crystals to perform *in situ* AFM characterization studies.

The authors acknowledge financial support from DGAPA (UNAM-México) grant No. IN204702. We also acknowledge the LUEP IQ-UNAM for providing us with the X-ray facilities and Dr Adela Rodríguez-Romero for her assistance during data collection. We thank Dr Alejandra Hernández-Santoyo for her assistance during the purification process and finally we thank Fís. Roberto Hernández for SEM and EDS technical assistance.

References

Granier, T., Gallois, B., Dautant, A., D'Estaintot, B. L. & Precigoux, G. (1997). *Acta Cryst.* D**53**, 580–587.
Harmer, M. A., Allen, H. & Hill, O. (1985). *J. Electroanal. Chem.* **189**, 229–246.
Olafson, R. W. (1988). *Bioelectrochem. Bioenerg.* **19**, 111–125.
Saeed, S. A. & Boyde, T. R. C. (1981). *FEBS Lett.* **123**, 111–114.
Sazaki, G., Moreno, A. & Nakajima, K. (2004). *J. Cryst. Growth*, **262**, 499–502.
Sazaki, G., Yoshida, E., Komatsu, H., Nakada, T., Miyashita, S. & Watanabe, K. (1997). *J. Cryst. Growth*, **173**, 231–234.
Theil, E. C. (2001). In *Handbook of Metalloproteins*, Vol. 2, edited by A. Messerschmidt, R. Huber, K. Weighardt & T. Poulos, pp. 771–781. Chichester: Wiley.
Tominaga, M., Ohira, A., Yamagushi, Y. & Masashi, T. (2004). *J. Electroanal. Chem.* **566**, 323–329.
Yau, S.-T. & Vekilov, P. G. (2001). *J. Am. Chem. Soc.* **123**, 1080–1089.